Journal of Advanced Research 24 (2020) 291–300

Contents lists available at ScienceDirect

Journal of Advanced Research

journal homepage: www.elsevier.com/locate/jare

Dietary lipids accumulate in macrophages and stromal cells and change the microarchitecture of mesenteric lymph nodes

Katharina Streich [a], Margarethe Smoczek [a,b], Jan Hegermann [c], Oliver Dittrich-Breiholz [d], Melanie Bornemann [e], Anja Siebert [a], Andre Bleich [a], Manuela Buettner [a,*]

[a] Institute of Laboratory Animal Science, Hannover Medical School, 30625 Hannover, Germany
[b] Institute for Neurophysiology, Hannover Medical School, 30625 Hannover, Germany
[c] Research Core Unit Electron Microscopy, Hannover Medical School, 30625 Hannover, Germany
[d] Research Core Unit Genomics, Hannover Medical School, 30625 Hannover, Germany
[e] Institute for Functional and Applied Anatomy, Hannover Medical School, 30625 Hannover, Germany

GRAPHICAL ABSTRACT

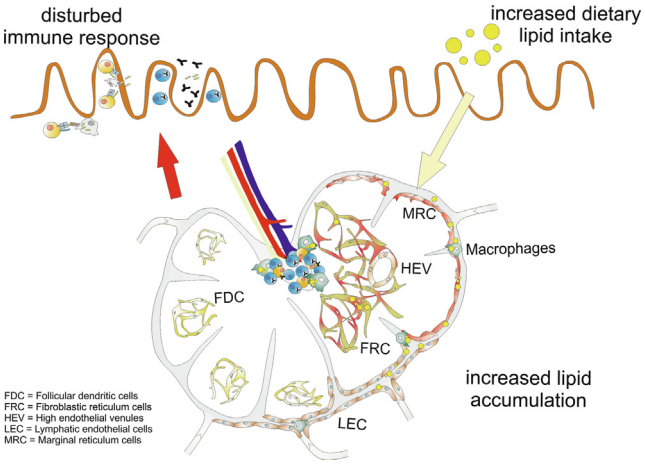

ARTICLE INFO

Article history:
Received 11 November 2019
Revised 24 April 2020
Accepted 28 April 2020
Available online 29 April 2020

Keywords:
Lipid droplets
Obesity
Lymphatic system
Microarray

ABSTRACT

In obesity, increased dietary lipids are taken up and transported by the lymphatic systems into the circulatory system. Increased fat accumulation results in impairments in the lymph fluid and lymph node (LN) atrophy. LNs filter the lymph fluid for foreign antigens to induce and control immune responses, and the alteration of this function during obesity remains underexplored. Here, the changes within the microarchitecture of mesenteric LNs (mLNs) during high levels of lipid transport were investigated, and the role of stromal cells in mice fed a high-fat diet for 10 weeks was assessed. Microarray experiments revealed that gene probes involved in lipid metabolism are expressed by mLN stromal cells. Transmission electron microscopy enabled the identification of lipid droplets in lymphatic endothelial cells, different reticulum cells, and macrophages, and the lipid droplet sizes as well as their numbers and intercellular distances increased after 10 weeks of high-fat diet feeding. The results indicate that

Peer review under responsibility of Cairo University.
* Corresponding author at: Institute for Laboratory Animal Sciences, Hannover Medical School, Carl-Neuberg-Str.1, 30625 Hannover, Germany.
E-mail address: Buettner.Manuela@mh-hannover.de (M. Buettner).

https://doi.org/10.1016/j.jare.2020.04.020
2090-1232/

changes in the microarchitecture and increased accumulation of lipid droplets in stromal cells and macrophages influence the immunological function of mLNs.

Introduction

Obesity is a worldwide health issue among children and adults [1]. Nutrients, including lipids, are absorbed in the intestine, particularly the jejunum, by enterocytes [2–4]. Short- and medium-chain fatty acids taken up from the diet are directly transported to the liver via the portal vein, whereas long-chain fatty acids are transformed into chylomicrons within enterocytes [5]. Chylomicrons enter the lymphatics and are transported into the blood [2,4]. In diet-induced obesity, lymphatic vessels and lymph fluid transport are impaired, which results in smaller draining lymph nodes (LNs) [6,7].

Mesenteric LNs (mLNs) drain the intestinal tract and form part of the immune system by activating and regulating immune cells during infection or inducing tolerance [8–10]. LNs are divided into different regions, such as the cortex, paracortex and medulla, and are surrounded and penetrated by lymph-filled sinuses [11]. These compartments are organized to manage a large number of motile lymphocytes (Ly) and antigen-presenting cells by resident stromal cells, including major types such as T-zone reticular cells (TRCs), follicular dendritic cells (FDCs), lymphatic endothelial cells (LECs) and blood endothelial cells (BECs) [12]. The afferent lymphatic vessels are connected to LNs and transport lymphoid fluid through the sinuses to the medulla, and the fluid exits through the efferent lymphatic vessels [13]. LECs express cytokines and chemokines, such as chemokine (C-C motif) ligand 21 (CCL21) and CCL19, to attract T cells, DCs, and adhesion molecules, such as platelet endothelial cell adhesion molecule 1 (PECAM-1) [14,15]. Therefore, LECs play a pivotal role in controlling transport and communication with immune cells [14]. However, particles smaller than 70 kDa or virions pass a filter built by LECs to enter the conduit system [16–18]. Conduits transport the filtered lymph through the paracortex to high endothelial venules (HEVs), where immune cells enter the LNs [19]. Although sheathed by TRCs, DCs can access the lumens of HEVs [20]. Thus, TRCs form a three-dimensional scaffold and influence the migration, survival, activation and function of lymphocytes [21–24]. TRCs express podoplanin (gp38) and extracellular matrix proteins such as ER-TR7. Single-cell RNA sequencing has revealed four distinct subtypes of TRCs, which are characterized by *Cxcl9*$^{+}$, *Ccl19*^{high}, *Ccl19*$^{+}$ and *Ccl19*$^{+}$*Il7*^{high} expression [25,26]. HEVs, which are found in the paracortex within the TRC network and the medulla [27], are specialized cuboidal endothelial cells that recruit Ly [28]. HEVs are impermeable to high-molecular-weight particles, but smaller particles reach paracortical and medullary HEVs through the conduit system [27]. Furthermore, capillary BECs are also detectable and provide nutrients and oxygen to the surrounding cells [28,29]. FDCs are located in the cortex, express CXCL13 for B cell migration and can function as antigen-presenting cells [30]. During immune reactions, FDCs remodel follicles into germinal centers, where B cells proliferate and undergo somatic hypermutations [30]. Because lipids are transported via lymph fluid through the mLNs, various cells are thought to come in contact with each other. Through high-resolution three-dimensional imaging, the transport route of lymph fluid, including a small tracer molecule, has been well illustrated, and the results have shown that all compartments come into contact with lymph-borne antigens [19]. The LN structure after high-fat diet (HFD) feeding has been analyzed, and this analysis revealed alterations and an abnormal organization [7,31] as well as decreased T cell numbers and increased cell death [7,32].

Thus, despite the occurrence of lipid transport and the induction of the immune response in mLNs, the microarchitecture of mLNs during obesity has not been widely explored. In the present study, animals were fed a HFD for 10 weeks, and transmission electron microscopy observations of these animals revealed various stromal cell subsets in most LN compartments and macrophages in contact with lipids. Furthermore, this study showed that stromal cells express high amounts of lipid metabolism-related genes, which indicated that mLNs participate in lipid metabolism.

Materials and methods

Mice and feeding

Five male mice per group (body weight, 18–25 g) were used in this study. C57BL/6NCrl (B6NCrl) mice were purchased from Charles River (Sulzfeld, Germany) and fed a HFD (D12492, Research Diets, New Brunswick, NJ, USA) containing 20% protein, 20% carbohydrate and 60% kcal fat or a low-fat diet (LFD; D12450J, Research Diets, New Brunswick, NJ, USA) containing 20% protein, 70% carbohydrate and 10% kcal fat ad libitum for 10–14 weeks. During the feeding period, the body weight was measured twice per week.

Ethical statement

This study was conducted in accordance with German animal protection laws and the European Directive 2010/63/EU. All the experiments were approved by the Local Institutional Animal Care and Research Advisory Committee and permitted by the Lower Saxony State Office for Consumer Protection and Food Safety (LAVES; file number: 13/1174).

Stromal cell (SC) isolation

For CD45^{-} SC isolation, mLNs or peripheral lymph nodes (pLNs) were obtained from the wild-type mice, and the LNs were digested at 37 °C for 30 min with 1 mg/ml collagenase 8 (Sigma-Aldrich, St. Louis, MO, USA) in RPMI 1640/10% FCS. The CD45^{-} cells were isolated using the MACS technique in accordance with the instructions provided by Miltenyi (Bergisch-Gladbach, Germany). The mean purity of the CD45^{-} cells from the mLN and pLN cells was 97.4% ± 2.0 and 97.5% ± 2.2, respectively, and that of the stromal cell subsets was 88% ± 1.5. The SCs were used for mRNA isolation.

Microarray analysis

The data discussed in this article have been deposited in NCBI's Gene Expression Omnibus [33] and are accessible under GEO SuperSeries accession number GSE138595 (https://www.ncbi.nlm.nih.gov/geo/query/acc.cgi?acc=GSE138595). All relevant laboratory processes and raw data processing steps are described in the database. For analysis and visualization, the normalized Processed Signals of the green channel (gPSs) were imported into

GeneSpring GX software (version 13.1.1, Agilent Technologies Inc., Santa Clara, CA, USA). The normalized values were imported as single-color data and log2-transformed according to the default import procedure. No additional data transformation or normalization was applied during the data import process.

Filter criteria for experiment #1 (pLNs versus mLNs): All the data were filtered to identify transcripts that fulfilled the following criteria: 1) fold difference in normalized gPSs calculated from both pairs of mLN vs pLN samples > 2-fold (consistent and unidirectional) and 2) an arithmetic mean of processed signal intensities calculated from both pairs of mLN vs pLN samples > 50.

Filter criteria for experiment #2 (mLN FRCs versus mLN LECs versus mLN BECs): All the data were filtered to identify transcripts that fulfilled the following criteria, which were applied separately for all possible pairwise comparisons (contrasts) among the three samples: 1) fold difference > 2-fold; 2) arithmetic mean of processed signal intensities calculated from both samples > 50; 3) absence (=0) of technical impairment, as defined by all four types of technical outliers (feature extraction software) in each of the samples analyzed.

Immunohistochemistry

Cryostat sections of mLNs were fixed in acetone/methanol solution (1:1, 10 min, −20 °C) and subjected to immunofluorescence histochemical analysis according to standard protocols. Briefly, the sections were rehydrated in TBST (0.1 M Tris pH 7.5, 0.15 M NaCl, and 0.1% Tween-20), preincubated with TBST containing 5% swine serum (Dako, Hamburg, Germany) and stained with antibodies against B220 and CD11b (BD Biosciences, Franklin Lakes, NJ, USA), CXCL13 (R&D Systems, Minneapolis, MN, USA), ERTR-7 (BMA, Augst, Switzerland), FDC-M1 (ImmunoKontact, Frankfurt, Germany), CD31-APC (BioLegend, San Diego, CA, USA) and Lyve-1 (kindly provided by R. Förster) in 2.5% serum/TBST. The unconjugated antibodies were then visualized using goat anti-rat Cy5 (Invitrogen, Carlsbad, CA, USA) or anti-rabbit Cy3 (Jackson ImmunoResearch, West Grove, PA, USA). The nuclei were visualized by DAPI staining (1 μg/ml DAPI/TBST), and the sections were mounted with Fluorescent Mounting Medium (Dako, Hamburg, Germany). Images were acquired using a Zeiss Axioskop 40 microscope (Carl Zeiss Microscopy GmbH, Göttingen, Germany) connected to an AxioCam MRm (Carl Zeiss, Göttingen, Germany).

Transmission electron microscopy

The mLNs were fixed by immersion in 150 mM HEPES, pH 7.35, containing 1.5% formaldehyde and 1.5% glutaraldehyde. After overnight incubation at 4 °C with 1% OsO_4 (2 h at RT) and 4% uranyl acetate, the mLNs were dehydrated in acetone and embedded in Epon. Subsequently, 50-nm sections were poststained with uranyl acetate and lead citrate (48) and observed with a Morgagni TEM (FEI, Eindhoven, Netherland). Images were captured with a side-mounted Veleta CCD camera (Olympus Soft Imaging Solutions, Münster, Deutschland).

Statistical analysis

All statistical analyses were performed using GraphPad Prism® 6 software (GraphPad Software, Inc., La Jolla, CA, USA). The data were tested for normality using the D'Agostino-Pearson ($n \geq 8$) normality test. For smaller sample sizes, the Shapiro-Wilk normality test ($n \geq 7$) or Kolmogorov-Smirnov test ($n \geq 5$) was used. The quantitative parametric data from two groups were compared using a *t* test. The significance level was set to 5%.

Results

Stromal cells express enzymes involved in lipid metabolism

Microarray analyses revealed significant differences in the expression patterns of several genes involved in lipid metabolism between pLN and mLN stromal cells. Genes such as *Clps* (colipase), *Pnlip* (pancreatic lipase), *Cpa1* (carboxypeptidase A1) and *Cel* (carboxyl ester lipase), which encode products involved in lipid metabolism, were more highly expressed in the stromal cells of mLNs than in those of pLNs (Fig. 1A, Suppl. Table 1). The analysis of different stromal cell subpopulations (FRC: $gp38^{+}CD31^{-}$; LEC: $gp38^{+}CD31^{+}$; BEC: $gp38^{-}CD31^{+}$; Suppl. Table 2) in a second microarray experiment showed high numbers of differentially expressed genes between FRCs and BECs (6886 gene probes), FRCs and LECs (5365 gene probes) and BECs and LECs (4269 gene probes). Fifty-one lipid metabolism-related gene probes representing 37 genes showed differential expression between FRCs and BECs, and 35 gene probes (27 genes) and 32 gene probes (27 genes) exhibited differential expression between FRCs and LECs and between BECs and LECs, respectively (Fig. 1B). The visualization of these genes in a scatter plot showed that BECs expressed a lower number of upregulated lipid metabolism-related genes compared with FRCs and LECs.

Increased sizes and numbers of lipid droplets in LECs and MRCs following HFD feeding

To determine whether stromal cells are in contact with dietary lipids, animals were fed a HFD (60%) or LFD (10%). After 10 weeks of feeding, the weight of the HFD-fed mice was 76% higher compared with that of the LFD-fed animals (Fig. 2). mLNs were isolated from these mice and analyzed by transmission electron microscopy to identify dietary lipids and determine the localization of lipid droplets (LDs). First, the analysis of the HFD group revealed increased LD numbers and sizes in various regions and cells of the mLNs (Fig. 2). A more detailed analysis provided insights into specific cell populations that are in contact with dietary lipids and into the localization of lipid vesicles within the different compartments of LNs.

The first region investigated in this study was the subcapsular sinus (SCS; Fig. 3A), where immune cells enter the lymph node from the draining area. LDs, Ly, dendritic cells (DCs) and mast cells (MCs) or macrophages (M) were detected within the SCS as well as in all other sinuses (intermediary and medullary) (Fig. 3B and 3C). Lymphocytes were identified by their round nucleus with dense chromatin and their small cytoplasm. DCs exhibited an irregular nucleus and several cytoplasmic protrusions but fewer lysosomes compared with macrophages. Macrophages were identified as large cells containing a nucleus with a peripheral rim of heterochromatin/condensed chromatin and a distinct nucleolus, and high numbers of granules and lysosomes were found within their cytoplasm. Furthermore, mast cells exhibited irregular nuclei and dark granules in the sinuses and particularly in the SCS of the LNs of LFD-fed mice, and reduced levels of these cells were found in the HFD-fed animals. In the LFD- and HFD-fed mice, macrophages were found loaded with lipids.

The SCS is lined by sessile nonhematopoietic stromal cells, namely, LECs and marginal reticulum cells (MRCs, Fig. 3D and E). LECs, which are flattened cells with an elongated nucleus, cover the SCS on two sites: the inner site flanking the cortex and the outer site next to the capsular region. The LECs facing the cortex were connected to collagen fibers and amorphous moderately electron-dense material. No or only some intracellular LDs and lysosome structures were found in the LECs of LFD-fed mice

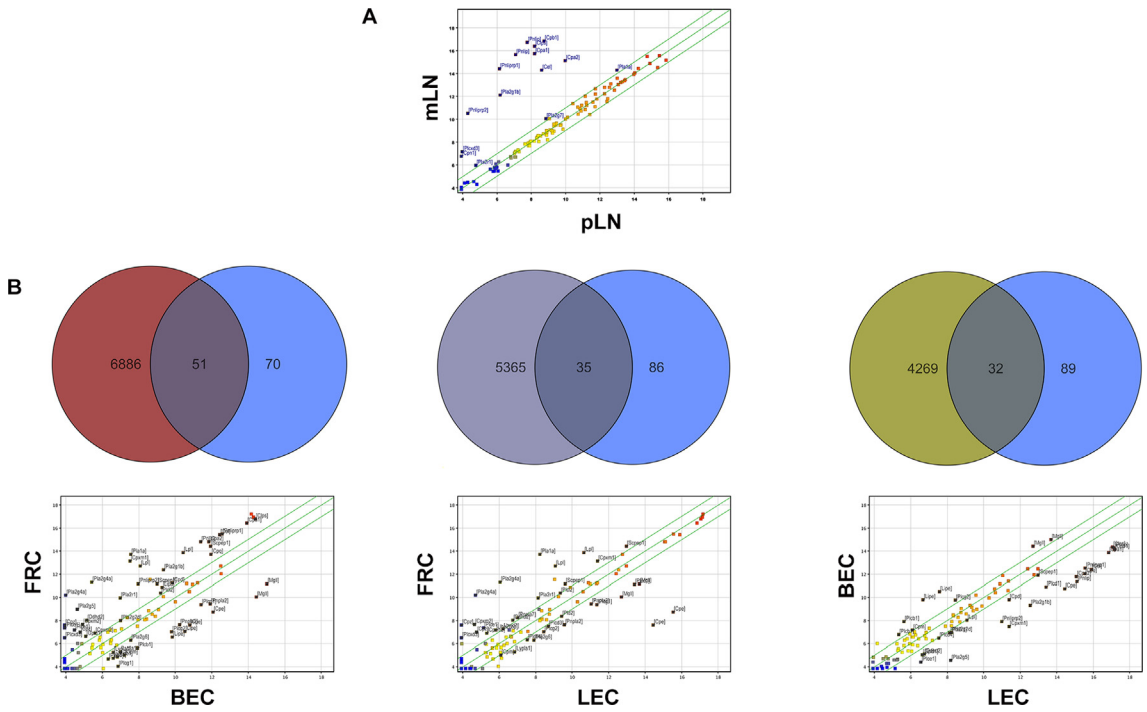

Fig. 1. Genes involved in lipid metabolism are expressed in mLN stromal cells, CD45⁻ SCs from mLNs and pLNs were isolated, and a microarray analysis was performed. A scatter plot analysis revealed that various lipid metabolism genes are upregulated in mLN stromal cells. (**B**) Subpopulations of mLN SCs were isolated within CD45⁻ cells. Using a combination of anti-CD31 and anti-gp38 antibodies, blood endothelial cells (BECs), lymph endothelial cells (LECs) and fibroblastic reticular cells (FRCs) were recognized. Genes encoding lipid metabolism components (blue circles) that fulfilled the applied filter criteria for differential mRNA expression and all the genes that showed altered expression between FRCs and BECs (red circle), FRCs and LECs (violet circle) or LECs and BECs (green circle) were analyzed using Venn diagrams. The lipid metabolism-related genes were further illustrated in scatter plots, and the differentially expressed genes are identified with gene symbols.

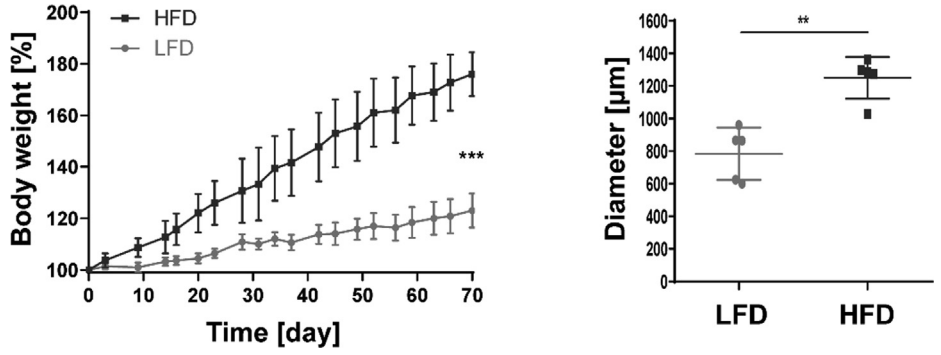

Fig. 2. HFD feeding increases the body weight and the number of lipid droplets in mLNs, The body weight of the mice after 10 weeks of LFD or HFD feeding was analyzed. The body weight (in %) was measured twice per week and calculated based on that at the initiation of LFD or HFD feeding (n = 3–5). The body weight at day 70 is shown. The lipid droplets throughout the mLN were measured (n = 5). Significant differences determined through an unpaired *t*-test are indicated by asterisks: ** P < 0.01; *** P < 0.001.

(Fig. 3D) and in the LECs on the capsular site of HFD-fed mice. In contrast, an increasing number of LDs were detected intracellularly in LECs on the inner site of the SCS after HFD feeding (Fig. 3E). LECs were found to be in direct contact with some type of sinusoidal reticular cell (SRC) in the sinuses and with MRCs at the outer layer of the cortex (Fig. 3D and E). These SRCs exhibited a light-colored nucleus/cytoplasm and numerous cell protrusions and cell organelles (Fig. 3E). However, MRCs showed a heterogeneous phenotype, as demonstrated by variations in both the shape and color of the cytoplasm. In addition, regardless of the diet, these cells exhibited an elongated, round or irregularly shaped pale nucleus, scattered Golgi complexes, and numerous mitochondria but only a few lysosomes. A normal morphology, including small LDs, was found in the MRCs of LFD-fed mice, whereas the LDs in the MRCs of the HFD-fed animals showed increases in both size and number (Suppl. Fig. 1).

Morphological changes in the interfollicular region following HFD feeding

The cortical area is divided into a follicular region (FR) and an interfollicular region (IFR) (Fig. 4A). Lymphoid follicles consist mostly of lymphocytes, but FDCs and macrophages could also be detected (Fig. 4B and C). FDCs were identified as large reticular cells with one or more light irregular nuclear profiles of finely dispersed chromatin. FDCs mainly occur in germinal centers of secondary follicles and exhibit numerous cytoplasmic protrusions. Within these germinal centers, tingible body macrophages with large phagolysosomes containing dead cells could also be identified. Lymphocytes and FDCs showed no morphological changes or intracellular LDs, regardless of the diet (Fig. 4B and 4C). In the IFR, some types of reticulum cells (now called interfollicular reticulum cells, IRCs) were observed in close proximity to the

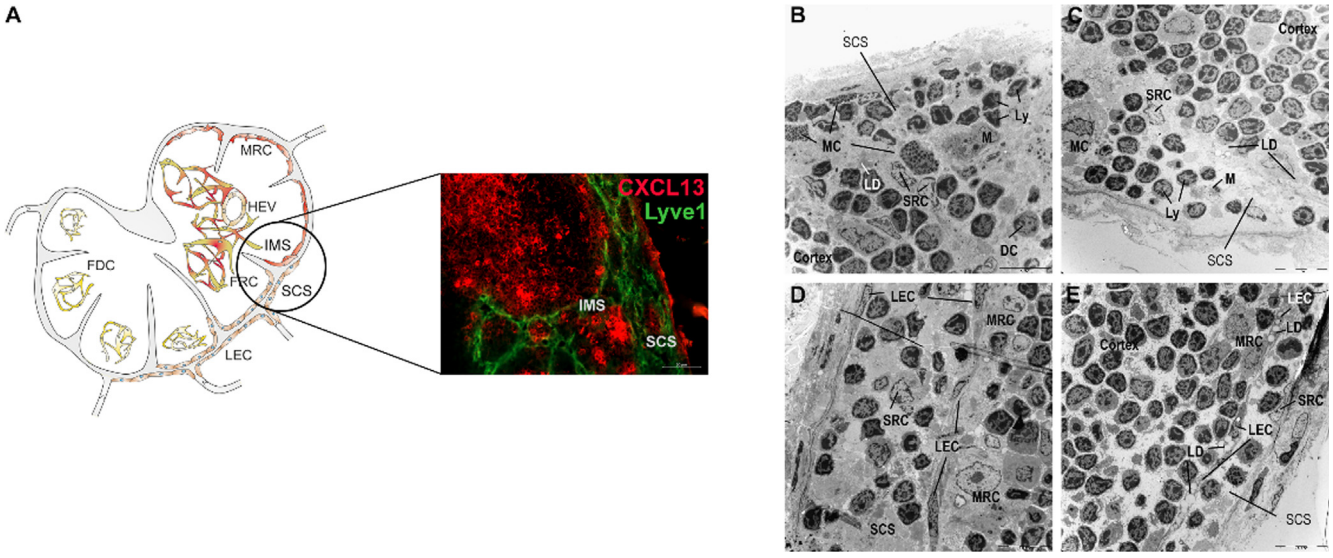

Fig. 3. Lipid droplets are present in lymphatic endothelial cells and marginal reticulum cells of the subcapsular sinus after HFD feeding, (**A**) Lymph endothelial cells (LECs, Lyve1$^+$) and marginal reticulum cells (MRCs, CXCL13$^+$) line up with the subcapsular sinus (SCS) of mLNs. (**B-E**) mLNs were isolated 10 weeks after LFD (**B, D**) or HFD (**C, E**) feeding, fixed and stained with uranyl acetate and lead citrate. Representative pictures (1.8 kx) of the subcapsular and intermediary sinuses are shown. Within the sinus, various mobile cell types (Ly, MCs, M, DCs) or LDs were identified. Abbreviations: DC, dendritic cell; FDC, follicular dendritic cell; FRC, fibroblastic reticulum cell; Ly, lymphocyte; M, macrophage; MC, mast cell; MRC, marginal reticulum cell; SCS, subcapsular sinus; and SRC, sinusoidal reticulum cell.

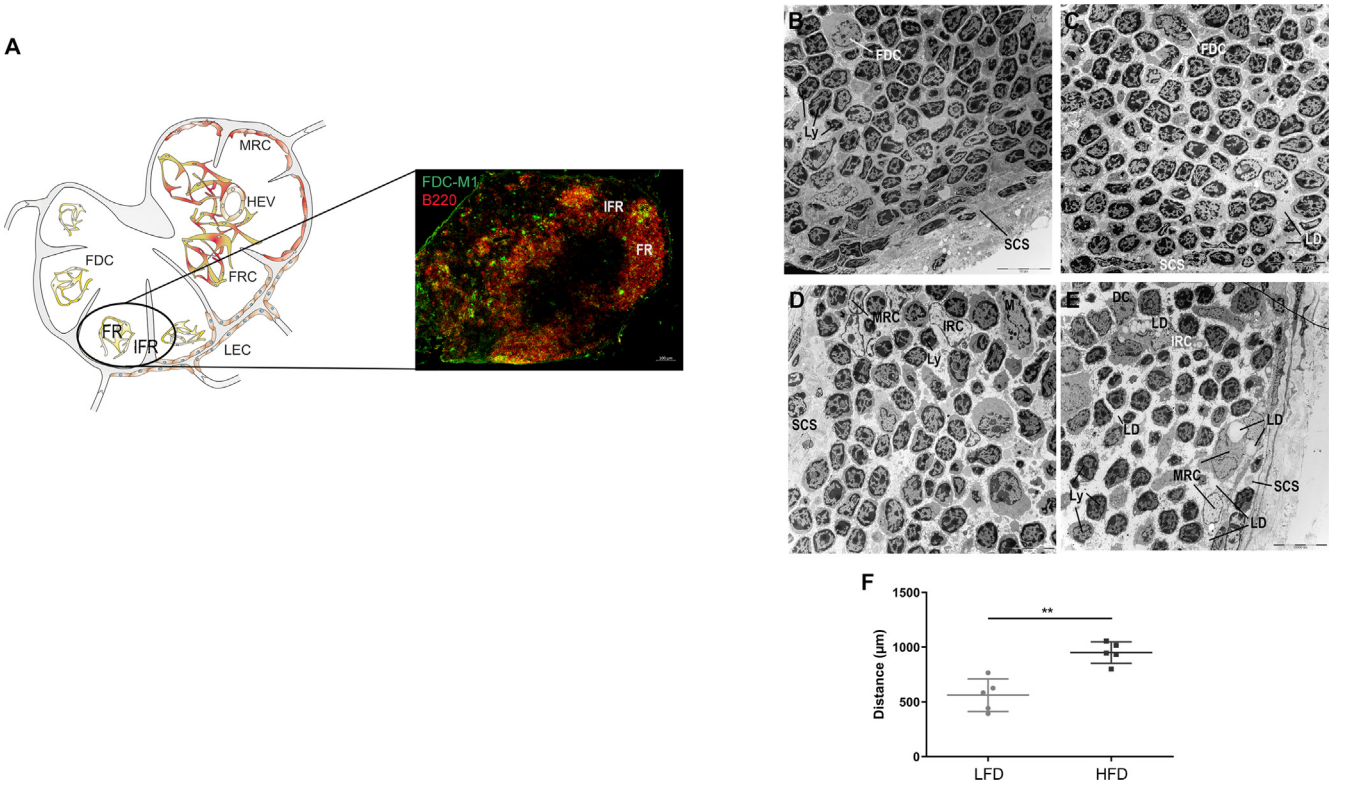

Fig. 4. Reticulum cells of the interfollicular region but not FDCs of the follicular region contain lipid droplets, (**A**) Follicular dendritic cells (FDCs, FDC-M1$^+$) are located in the B cell (B220$^+$) area of mLNs. (**B-F**) mLNs were isolated, fixed and stained with uranyl acetate and lead citrate 10 weeks after LFD (**B, D**) or HFD (**C, E**). Representative pictures (1.8 kx) of the cortex are shown. Lymphocytes and FDCs were detected within the follicular regions (**B, C),** and interfollicular reticulum cells, dendritic cells or lipid droplets were identified within the interfollicular region **(D, E)**. (**F**) The intercellular distances between cells were measured (n = 5). Significant differences determined using an unpaired *t*-test are indicated by asterisks: ** P < 0.01. Abbreviations: DC, dendritic cell; FDC, follicular dendritic cell; FR, follicular region; FRC, fibroblastic reticulum cell; HEV, high endothelial venules; IFR, interfollicular region; IRC, interfollicular reticulum cell; LD, lipid droplet; LEC, lymphatic endothelium cell; Ly, lymphocyte; MRC, marginal reticulum cell; and SCS, subcapsular sinus.

intermediary/cortical sinuses (Fig. 4D and 4E). These cells exhibited a fusiform structure and an irregularly shaped nucleus with a peripheral rim of dense chromatin and were in direct contact with lymphocytes, macrophages and DCs. LDs in the cytoplasm of these IRCs were observed only in the HFD-fed mice (Fig. 4E). Furthermore, in this region, some free LDs in the interstitium and larger intercellular spaces were observed in the HFD-fed mice compared with the LFD-fed mice (Fig. 4F).

Lipid droplets do not enter the paracortex

The paracortex was characterized by the presence of HEVs, lymphocytes, DCs and FRCs (Fig. 5A-5E). The HEVs were constructed by BECs and were surrounded by reticular fibers and pericytes (Fig. 5-B-5E). These specialized postcapillary venules represent the portals for the entry of lymphocytes migrating from the bloodstream into the LNs. Subsequently, the HEV FRCs formed a three-dimensional network (conduit) in which various FRCs were connected via their cytoplasmic extensions (Fig. 5B and 5C). These reticular cells showed a fusiform or stellate-shaped structure, a dark cytoplasm due to irregularly distributed strands of the endoplasmic reticulum, and a long ovoid nucleus. In addition, these cells were highly connected to collagen fibers, and DCs and lymphocytes were found to be in close contact with FRCs. Morphological changes or LDs were not observed in this region of the paracortex. However, in the paracorticomedullary transition area, the FRCs of the LFD-fed mice exhibited small intracellular LDs (Fig. 5F, Suppl. Fig. 2), and highest numbers of and larger LDs were found in the HFD-fed mice (Fig. 5G).

Stromal cells but not leucocytes integrate lipid droplets in the medulla

The last compartment of the LN is the medulla (Fig. 6A). This region consists of medullary sinuses and cords, and blood vessels could also be detected. The medullary sinuses are lined with SRCs and LECs (Fig. 6B and 6C). The cords contain plasma cells, lymphocytes and macrophages between some RCs and FRCs (Fig. 6D and 6E). Plasma cells possess a pronounced, occasionally dilated rough endoplasmic reticulum and a round nucleus. Neither these antibody-producing cells nor the other leucocytes showed morphological changes between the different groups. Furthermore, independent of the diet, apoptotic cells were observed mostly near blood vessels in the interstitium of this region. These cells were characterized by condensation of chromatin and fragmentation of the nucleus and many autolysosomes, including cell debris. Similar to the results obtained in the paracorticomedullary area, small LDs were noted in FRCs surrounding the blood vessels in the LFD-fed mice and were increased in the HFD-fed mice at the end of the 10-week feeding period (Fig. 6B and C). Moreover, intracellular LDs were observed in SRCs of HFD-fed mice (Fig. 6C).

Lipophages and foam cells are detected in the sinuses after HFD feeding

Additionally, macrophages representing only a small cell population in the LNs were detected in all sinuses of the LFD-fed mice and in the mLNs of HFD-fed mice, starting from the SCS to the cortical sinus and converging in the medulla (Figs. 3B, C, and 7A-C). Typical sinus macrophages contain many different types of lysosomes. In the medullary sinuses, macrophages showed an increased number of bright heterolysosomes (HLs) containing lipids or chylomicrons and were therefore called lipophages (Figs. 6B, 7C and D). However, following HFD feeding, enlarged numbers of these lipophages were identified within the intermediary/cortical and medullary sinuses (Fig. 7C). Furthermore,

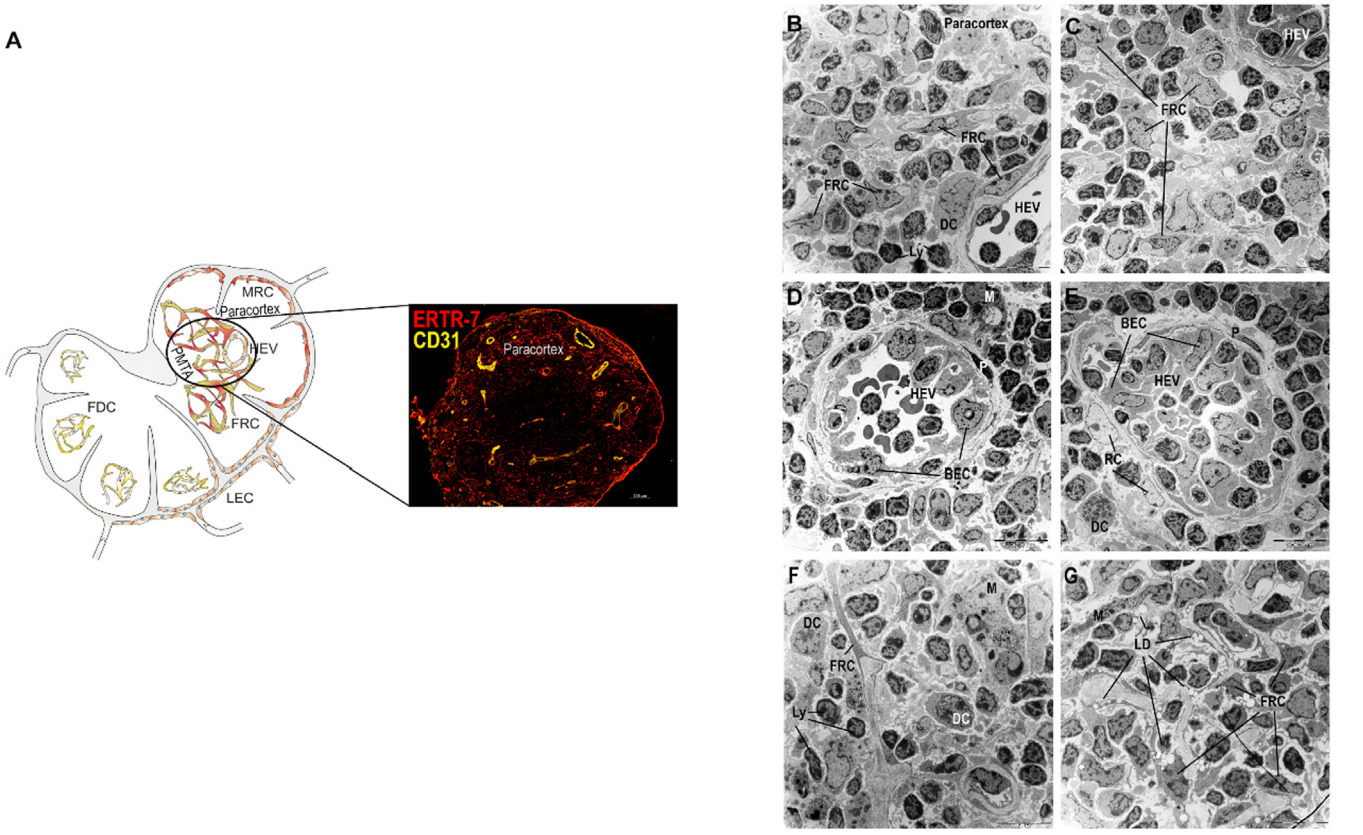

Fig. 5. Lipid droplets are present only in the paracorticomedullary transition area, (**A**) Fibroblastic reticulum cells (FRCs, ERTR7$^+$) and high endothelial venules (HEVs, CD31$^+$) are located in the paracortex of mLNs. mLNs were isolated 10 weeks after LFD (**B, D, F**) or HFD (**C, E, G**) feeding, fixed and stained with uranyl acetate and lead citrate. Representative pictures (1.8 kx) of the paracortex are shown. Within the T cell region (**B-E**), lymphocytes, FRCs, dendritic cells and HEVs were identified. (**D, E**) HEVs were built by blood endothelial cells and surrounded by pericytes and reticulum cells. No lipid droplets were detectable in this region. (**F, G**) Within the paracorticomedullary transition area, FRCs carrying lipid droplets and intercellular lipid droplets were detected after HFD feeding. Abbreviations: BEC, blood endothelial cell; DC, dendritic cell; FDC, follicular dendritic cell; FRC, fibroblastic reticulum cell; HEV, high endothelial venule; LD, lipid droplet; LEC, lymphatic endothelium cell; Ly, lymphocyte; M, macrophage; MRC, marginal reticulum cell; P, pericyte; PMTA, paracorticomedullary transition area; and RC, reticulum cell.

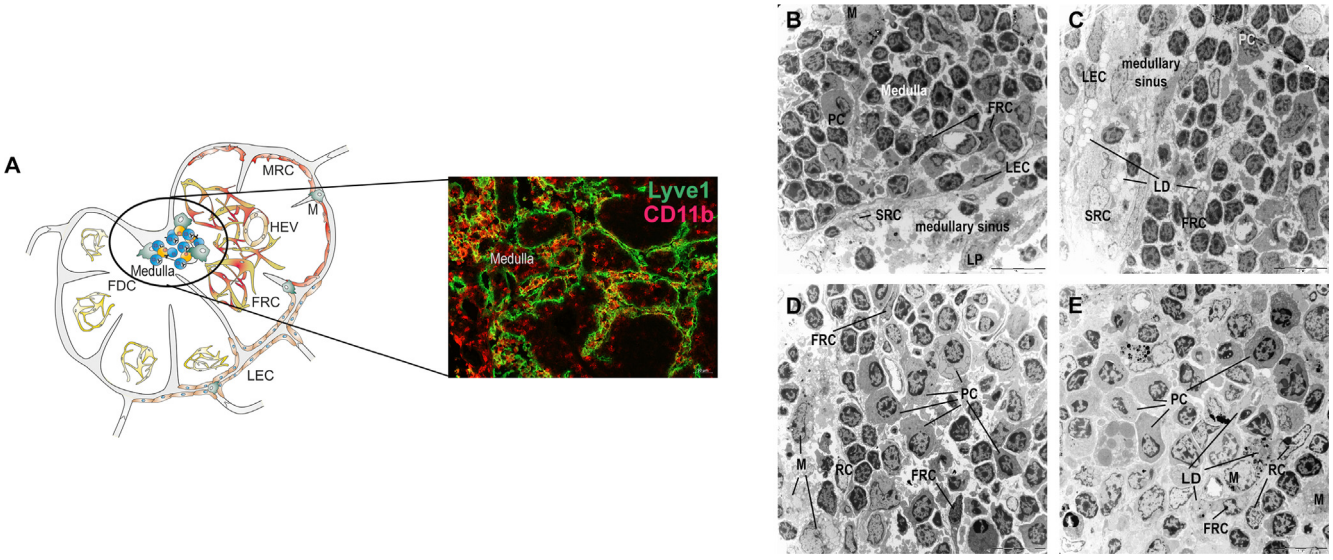

Fig. 6. Lipid droplets are detectable in stromal cells of the medulla, (**A**) Lymph endothelial cells (LECs, Lyve1$^+$), plasma cells, T cells and B cells as well as macrophages (M, CD11b$^+$) are present in the medullary region of mLNs. mLNs were isolated 10 weeks after LFD (**B, D**) or HFD (**C, E**) feeding, fixed and stained with uranyl acetate and lead citrate. Representative pictures (1.8 kx) of the medulla and the medullary sinus are shown. Lymphocytes, plasma cells, and macrophages as mobile cells and sinusoidal reticulum cells, lymph endothelial cells, reticulum cells and FRCs as sessile cells were identified. Lipid droplets were detected in mLNs after HFD feeding. Abbreviations: FDC, follicular dendritic cell; FRC, fibroblastic reticulum cell; HEV, high endothelial venule; LD, lipid droplet; LEC, lymphatic endothelium cell; LP, lipophage; M, macrophage; MRC, marginal reticulum cell; PC, plasma cell; RC, reticulum cell; and SRC, sinusoidal reticulum cell.

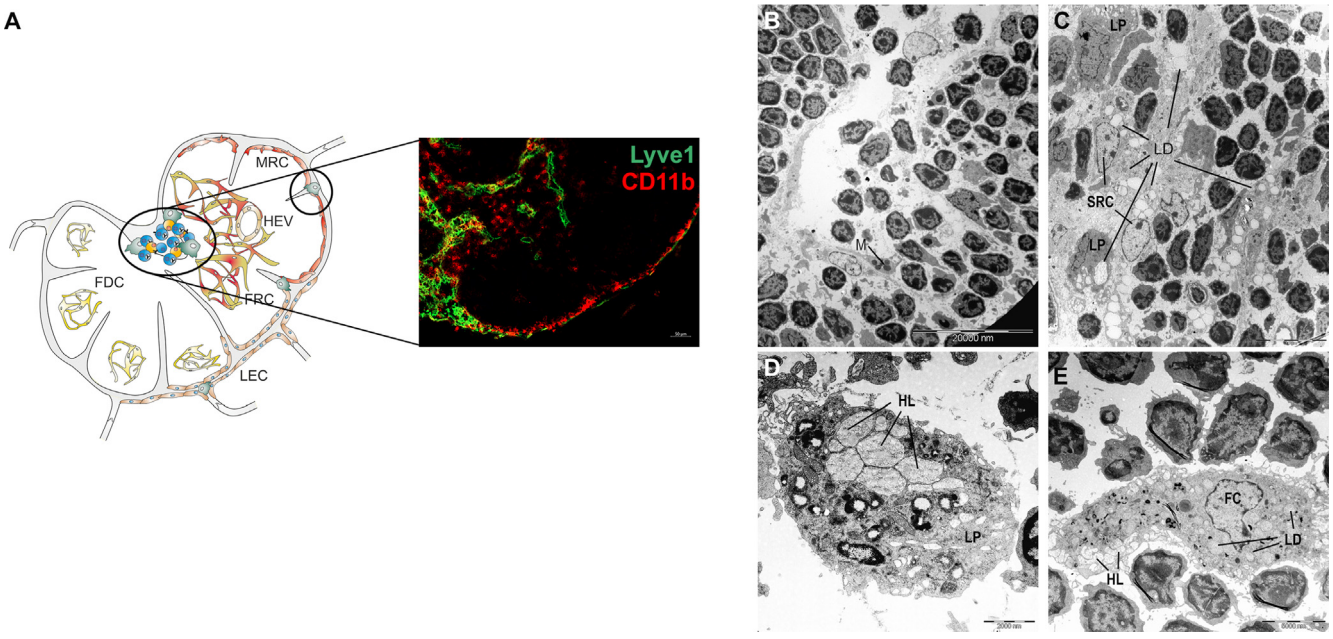

Fig. 7. Macrophages in all regions of mLNs incorporate lipid droplets, (A) Macrophages (M, CD11b$^+$) are present in all sinuses and the medullary region of mLNs. (**B-E**) mLNs were isolated 10 weeks after LFD (**B**) or HFD (**C-E**) feeding, fixed and stained with uranyl acetate and lead citrate. Representative pictures (1.8 kx) of the intermediary sinus are shown. (**C**) In all regions, macrophages carried increased numbers of lipid droplets of larger sizes after HFD feeding. (**D**) Lipophages (8.9 kx) showing heterolysosomes (HL) were detected in mLNs, independent of the diet, whereas foam cells (7.8 kx) were found in mLNs only after HFD feeding (**E**). Abbreviations: FC, foam cell; FDC, follicular dendritic cell; FRC, fibroblastic reticulum cell; HEV, high endothelial venule; HL, heterolysosome; LD, lipid droplet; LEC, lymphatic endothelium cell; LP, lipophage; M, macrophage; MRC, marginal reticulum cell; and SRC, sinusoidal reticulum cell.

macrophages that transformed into foam cells could be detected, and these showed increased intracytoplasmic LDs in addition to HLs (Fig. 7E).

Discussion

Increased dietary fat intake leads to the accumulation of dietary lipids, and the dysregulation of lipid metabolism during obesity exerts several effects on different organs [34–36]. Dietary lipids pass the mLNs during their transport by afferent lymphatics from the small intestine to the thoracic duct. The direct contact between mLN cells and dietary lipids suggests the involvement of mLNs in lipid metabolism. Furthermore, mLNs form part of the intestinal immune system and maintain inner homeostasis by generating immune responses against potential pathogens or pathologically altered cells and inducing tolerance against harmless antigens

[12]. This study showed that the mLN is affected during obesity and that most stromal cells and macrophages store high amounts of LDs.

In recent years, scientists have focused on the stromal cells of LNs because these cells are involved in immunological functions, such as the immune response and tolerance induction [12]. Different types of stromal cells, such as FDCs and FRCs, were detected in the follicles or T cell zone of the LNs, respectively. Together with LECs and BECs, these stromal cell subpopulations were sorted and analyzed based on their gene expression profiles [22,24]. mLNs and pLNs share similar gene expression profiles within these clusters, such as genes belonging to the interferon family, *Ccl19* and *Ccl21*, but also show differences, such as in the expression of *Il6* or *Cxcl14* [22,24]. However, differences between the LNs and stromal cell subpopulations were detected. *Il7*, as a lymphocyte survival-related cytokine, exhibits markedly higher expression in FRCs than in BECs [24]. Many more stromal cell subsets were recently identified by single-cell sequencing, and these findings resulted in the identification of four FRC subtypes ($Cxcl9^+$, $Ccl19^{high}$, $Ccl19^+$ and $Ccl19^+Il7^{high}$ TRCs) or the identification of new stromal cell populations, such as $CD34^+$ cells. These cells could be subdivided into $CD34^+(Aldh1a2^+)$, $CD34^+(Ackr3^+)$, $CD34^+(Gdf10^+)$ and $CD34^+(Cd248^+)$ SCs [25,26], and all these stromal cell populations exhibited a distinct gene expression profile. This study revealed that a substantial number of genes involved in lipid metabolism exhibited increased expression in mLN stromal cells compared with pLN stromal cells. Dietary lipids are absorbed in the intestine and transported via afferent lymphatics to the mLNs and then to the thoracic duct [2]. Therefore, mLNs but not pLNs are in contact with these lipids. These results suggest that mLNs play a role in lipid metabolism. The gene expression of these enzymes in the stromal cell subpopulation of the mLNs was examined, and genes involved in lipid metabolism were detected in all analyzed subpopulations (FRCs, BECs and LECs). In addition, the highest number of upregulated genes were found in FRCs. Prior to this study, scarce information on lipid metabolism or lipid accumulation in mLNs is available. Therefore, mice were fed an LFD or HFD, and the morphological differences and lipid-cell interactions in their mLNs were analyzed. LDs were identified predominantly in or near the sinuses, the paracorticomedullary transition area and the medulla after 10 weeks of HFD feeding.

The lymphoid fluid is transported through afferent lymphatic vessels to the mLNs and SCS, which is lined with LECs. LECs, which are characterized by LYVE1 expression, control the entrance of lymphocytes [37]. Furthermore, LECs transport extracellular proteins and soluble substances [38] and filter particles smaller than 70 kDa or virions [16–18]. Two other stromal cell populations (MRCs and $CD34^+$ SCs) are located below the SCS [26,39,40], and both of these cell types are thought to play a role in capsule integrity and are in direct contact with LECs [26]. This study identified two different stromal cell populations attached to LECs: one cell population was identified as MRCs, and the other cell population was termed SRCs. These cells, which might be $CD34^+$ SCs, are direct contact with the lymph fluid, whereas the cells in the cortex and paracortex are connected to filtered lymph fluid via the conduit system [17,19,20]. Increased numbers of LDs of increased sizes were detected in LECs, MRCs and SRCs in all sinuses (the SCS, intermediary and medullary sinuses) after 10 weeks of HFD feeding, whereas the FDCs in the follicular region and TRCs in the paracortical area did not contain LDs in their cytoplasm. FDCs are known to capture and present antigens [41], and $Ccl19^{high}$ TRCs build and envelope the conduit system [20]. These cells express high levels of *Ccl21* in addition to *Ccl19* [42], cytokines needed for T and B cell survival, such as *Il7* and *Baff*, [42,43], and pattern recognition receptors to control innate immune responses [44,45] and present self-antigens via peptide-MHCII complexes to tolerize T cells [46,47]. In addition, reticulum cells surrounding HEVs and HEV endothelial cells were also found to lack LDs. HEVs are considered the entrance points for lymphocytes from the circulation to the paracortical regions of the LNs [12]. Thus, the dietary lipids obtained from HFD consumption appear to be mostly filtered by LECs and are not transported via the conduit system to the paracortical area. However, in the interfollicular zone, LDs were observed in the cytoplasm of IRCs in the HFD-fed mice, and some free LDs were detected in the interstitium. These cells are in direct contact with lymphocytes, macrophages and DCs. This region has been described as the primary site for stromal cell-DC-T cell interactions [48] and the activation of antigen-specific T cells [18]. Therefore, the larger intercellular spaces observed in the HFD-fed mice compared with those observed in the LFD-fed mice might be important for induction of the immune response in this region. A topological analysis of the T cell zone (TCZ) showed that lymphocytes in the superficial TCZ are in continuous contact with the conduit network and therefore with FRCs [19]. The altered microarchitecture due to an increased collagen content or increased cell debris within the paracortex [31] and the increased apoptosis of activated T cells [32] support the hypothesis that obesity results in mLNs that show an impaired immune function. Furthermore, the mice showed smaller mLNs and reduced lymph vessels after consumption of the HFD [7], which mimics the clinical symptoms observed in obese patients developing lymphedema [49].

The medulla, where lymphocytes exit via efferent lymphatics, consists of medullary cords and lymph sinuses [50]. In addition to all lymphocyte subtypes, such as B and T cells or plasma cells, which leave the LNs, various types of stromal cells, such as nondifferentiated reticular cells, medullary zone FRCs, phagocytic reticular cells, $CD34^+$ stromal cells and LECs, were detected in this region [23,26,51–53]. In this study, stromal cells but not leucocytes were found to contain LDs. Additionally, macrophages were located in both the medulla and the SCS. Although all of these cells phagocytose antigens and present them to lymphocytes for immune response induction, SCS macrophages exhibit less efficient phagocytosis but more efficient virus capture [54]. Independent of the diet, macrophages can be distinguished from lipophages in the sinuses of the mLNs by the presence of increased lipids or chylomicrons in heterolysosomes. However, foam cells containing LDs within their cytoplasm were detected only in the mLNs of the HFD-fed mice. Lipophages express the enzyme lipoprotein lipase, which catalyzes the hydrolysis of chylomicrons [55,56], whereas foam cells are formed by high-lipid material exposure and are characteristic of lipid lymphadenopathy [57].

Conclusion

In conclusion, this study provides the first demonstration that stromal cells and macrophages are almost exclusively involved in lipid uptake in the mLNs. Because all of these cells are involved in immune response induction or homeostasis maintenance, it is possible that a high lipid intake, lipid transport through the sinuses of the LNs and lipid absorption by the cells impair their immunological function.

Declaration of Competing Interest

The authors declare that they have no known competing financial interests or personal relationships that could have appeared to influence the work reported in this paper.

Acknowledgments

We thank Anna Smoczek and Andrea Liese for their excellent technical assistance. We would also like to acknowledge the assistance of the Cell Sorting Core Facility of the Hannover Medical School funded in part by the Braukmann-Wittenberg-Herz-Stif tung and the Deutsche Forschungsgemeinschaft. The work was supported by the German Research Foundation (BO 1866/3-1).

Appendix A. Supplementary material

Supplementary data to this article can be found online at https://doi.org/10.1016/j.jare.2020.04.020.

References

[1] Goossens GH. The metabolic phenotype in obesity: fat mass, body fat distribution, and adipose tissue function. Obes Facts 2017;10(3):207–15.
[2] Klop B, Elte JW, Cabezas MC. Dyslipidemia in obesity: mechanisms and potential targets. Nutrients 2013;5(4):1218–40.
[3] Wang TY, Liu M, Portincasa P, Wang DQ. New insights into the molecular mechanism of intestinal fatty acid absorption. Eur J Clin Invest 2013;43 (11):1203–23.
[4] Beilstein F, Carriere V, Leturque A, Demignot S. Characteristics and functions of lipid droplets and associated proteins in enterocytes. Exp Cell Res 2016;340 (2):172–9.
[5] Schonfeld P, Wojtczak L. Short- and medium-chain fatty acids in energy metabolism: the cellular perspective. J Lipid Res 2016;57(6):943–54.
[6] Blum KS, Karaman S, Proulx ST, Ochsenbein AM, Luciani P, Leroux JC, et al. Chronic high-fat diet impairs collecting lymphatic vessel function in mice. PLoS ONE 2014;9(4):e94713.
[7] Weitman ES, Aschen SZ, Farias-Eisner G, Albano N, Cuzzone DA, Ghanta S, et al. Obesity impairs lymphatic fluid transport and dendritic cell migration to lymph nodes. PLoS ONE 2013;8(8):e70703.
[8] Worbs T, Bode U, Yan S, Hoffmann MW, Hintzen G, Bernhardt G, et al. Oral tolerance originates in the intestinal immune system and relies on antigen carriage by dendritic cells. J Exp Med 2006;203(3):519–27.
[9] Yero A, Farnos O, Rabezanahary H, Racine G, Estaquier J, Jenabian MA. Differential dynamics of regulatory T-cell (Treg) and Th17 cell balance in mesenteric lymph nodes and blood following early anti-retroviral initiation during acute SIV infection. J Virol 2019;93(19):e00371–e419.
[10] Hahn A, Thiessen N, Pabst R, Buettner M, Bode U. Mesenteric lymph nodes are not required for an intestinal immunoglobulin A response to oral cholera toxin. Immunology 2010;129(3):427–36.
[11] Van den Broeck W, Derore A, Simoens P. Anatomy and nomenclature of murine lymph nodes: Descriptive study and nomenclatory standardization in BALB/cAnNCrl mice. J Immunol Methods 2006;312(1–2):12–9.
[12] Chang JE, Turley SJ. Stromal infrastructure of the lymph node and coordination of immunity. Trends Immunol 2015;36(1):30–9.
[13] Mueller SN, Germain RN. Stromal cell contributions to the homeostasis and functionality of the immune system. Nat Rev Immunol 2009;9 (9):618–29.
[14] Farnsworth RH, Karnezis T, Maciburko SJ, Mueller SN, Stacker SA. The Interplay Between Lymphatic Vessels and Chemokines. Front Immunol 2019;10:518.
[15] Sawa Y, Yoshida S, Ashikaga Y, Kim T, Yamaoka Y, Shiroto H. Lymphatic endothelium expresses PECAM-1. Tissue Cell 1998;30(3):377–82.
[16] Rantakari P, Auvinen K, Jappinen N, Kapraali M, Valtonen J, Karikoski M, et al. The endothelial protein PLVAP in lymphatics controls the entry of lymphocytes and antigens into lymph nodes. Nat Immunol 2015;16 (4):386–96.
[17] Roozendaal R, Mebius RE, Kraal G. The conduit system of the lymph node. Int Immunol 2008;20(12):1483–7.
[18] Reynoso GV, Weisberg AS, Shannon JP, McManus DT, Shores L, Americo JL, et al. Lymph node conduits transport virions for rapid T cell activation. Nat Immunol 2019;20(5):602–12.
[19] Kelch ID, Bogle G, Sands GB, Phillips ARJ, LeGrice IJ, Dunbar PR. High-resolution 3D imaging and topological mapping of the lymph node conduit system. PLoS Biol 2019;17(12):e3000486.
[20] Sixt M, Kanazawa N, Selg M, Samson T, Roos G, Reinhardt DP, et al. The conduit system transports soluble antigens from the afferent lymph to resident dendritic cells in the T cell area of the lymph node. Immunity 2005;22 (1):19–29.
[21] Buettner M, Pabst R, Bode U. Lymph node stromal cells strongly influence immune response suppression. Eur J Immunol 2011;41(3):624–33.
[22] Buettner M, Dittrich-Breiholz O, Falk CS, Lochner M, Smoczek A, Menzel F, et al. Stromal cells as trend-setters for cells migrating into the lymph node. Mucosal Immunol 2015;8(3):640–9.
[23] Huang HY, Rivas-Caicedo A, Renevey F, Cannelle H, Peranzoni E, Scarpellino L, et al. Identification of a new subset of lymph node stromal cells involved in regulating plasma cell homeostasis. Proc Natl Acad Sci USA 2018;115(29): E6826–35.
[24] Malhotra D, Fletcher AL, Astarita J, Lukacs-Kornek V, Tayalia P, Gonzalez SF, et al. Transcriptional profiling of stroma from inflamed and resting lymph nodes defines immunological hallmarks. Nat Immunol 2012;13 (5):499–510.
[25] Pezoldt J, Pasztoi M, Zou M, Wiechers C, Beckstette M, Thierry GR, et al. Neonatally imprinted stromal cell subsets induce tolerogenic dendritic cells in mesenteric lymph nodes. Nat Commun 2018;9(1):3903.
[26] Rodda LB, Lu E, Bennett ML, Sokol CL, Wang X, Luther SA, et al. Single-Cell RNA Sequencing of Lymph Node Stromal Cells Reveals Niche-Associated Heterogeneity. Immunity 2018;48(5). pp. 1014–28 e6.
[27] Pfeiffer F, Kumar V, Butz S, Vestweber D, Imhof BA, Stein JV, et al. Distinct molecular composition of blood and lymphatic vascular endothelial cell junctions establishes specific functional barriers within the peripheral lymph node. Eur J Immunol 2008;38(8):2142–55.
[28] Girard JP, Springer TA. High endothelial venules (HEVs): specialized endothelium for lymphocyte migration. Immunol Today 1995;16(9):449–57.
[29] Anderson ND, Anderson AO, Wyllie RG. Specialized structure and metabolic activities of high endothelial venules in rat lymphatic tissues. Immunology 1976;31(3):455–73.
[30] Gentek R, Bajenoff M. Lymph Node Stroma Dynamics and Approaches for Their Visualization. Trends Immunol 2017;38(4):236–47.
[31] Solt CM, Hill JL, Vanderpool K, Foster MT. Obesity-induced immune dysfunction and immunosuppression: TEM observation of visceral and subcutaneous lymph node microarchitecture and immune cell interactions. Horm Mol Biol. Clin Investig. 2019;39(2). /j/hmbci.2019.39.issue-2/hmbci-2018-0083/hmbci-2018-0083.xml.
[32] Kim CS, Lee SC, Kim YM, Kim BS, Choi HS, Kawada T, et al. Visceral fat accumulation induced by a high-fat diet causes the atrophy of mesenteric lymph nodes in obese mice. Obesity (Silver Spring). 2008;16(6):1261–9.
[33] Edgar R, Domrachev M, Lash AE. Gene Expression Omnibus: NCBI gene expression and hybridization array data repository. Nucleic Acids Res 2002;30 (1):207–10.
[34] Auclair N, Melbouci L, St-Pierre D, Levy E. Gastrointestinal factors regulating lipid droplet formation in the intestine. Exp Cell Res 2018;363(1):1–14.
[35] Magnuson AM, Regan DP, Booth AD, Fouts JK, Solt CM, Hill JL, et al. High-fat diet induced central adiposity (visceral fat) is associated with increased fibrosis and decreased immune cellularity of the mesenteric lymph node in mice. Eur J Nutr 2019. doi: https://doi.org/10.1007/s00394-019-02019-z.
[36] Olzmann JA, Carvalho P. Dynamics and functions of lipid droplets. Nat Rev Mol Cell Biol 2019;20(3):137–55.
[37] Ulvmar MH, Werth K, Braun A, Kelay P, Hub E, Eller K, et al. The atypical chemokine receptor CCRL1 shapes functional CCL21 gradients in lymph nodes. Nat Immunol 2014;15(7):623–30.
[38] Triacca V, Guc E, Kilarski WW, Pisano M, Swartz MA. Transcellular Pathways in Lymphatic Endothelial Cells Regulate Changes in Solute Transport by Fluid Stress. Circ Res 2017;120(9):1440–52.
[39] Katakai T, Suto H, Sugai M, Gonda H, Togawa A, Suematsu S, et al. Organizer-like reticular stromal cell layer common to adult secondary lymphoid organs. J Immunol 2008;181(9):6189–200.
[40] Sitnik KM, Wendland K, Weishaupt H, Uronen-Hansson H, White AJ, Anderson G, et al. Context-Dependent Development of Lymphoid Stroma from Adult CD34(+) Adventitial Progenitors. Cell Rep. 2016;14(10):2375–88.
[41] Suzuki K, Grigorova I, Phan TG, Kelly LM, Cyster JG. Visualizing B cell capture of cognate antigen from follicular dendritic cells. J Exp Med 2009;206 (7):1485–93.
[42] Link A, Vogt TK, Favre S, Britschgi MR, Acha-Orbea H, Hinz B, et al. Fibroblastic reticular cells in lymph nodes regulate the homeostasis of naive T cells. Nat Immunol 2007;8(11):1255–65.
[43] Cremasco V, Woodruff MC, Onder L, Cupovic J, Nieves-Bonilla JM, Schildberg FA, et al. B cell homeostasis and follicle confines are governed by fibroblastic reticular cells. Nat Immunol 2014;15(10):973–81.
[44] Gil-Cruz C, Perez-Shibayama C, Onder L, Chai Q, Cupovic J, Cheng HW, et al. Fibroblastic reticular cells regulate intestinal inflammation via IL-15-mediated control of group 1 ILCs. Nat Immunol 2016;17(12):1388–96.
[45] Gregory JL, Walter A, Alexandre YO, Hor JL, Liu R, Ma JZ, et al. Infection Programs Sustained Lymphoid Stromal Cell Responses and Shapes Lymph Node Remodeling upon Secondary Challenge. Cell Rep 2017;18(2):406–18.
[46] Baptista AP, Roozendaal R, Reijmers RM, Koning JJ, Unger WW, Greuter M, et al. Lymph node stromal cells constrain immunity via MHC class II self-antigen presentation. Elife 2014;3.
[47] Dubrot J, Duraes FV, Potin L, Capotosti F, Brighouse D, Suter T, et al. Lymph node stromal cells acquire peptide-MHCII complexes from dendritic cells and induce antigen-specific CD4(+) T cell tolerance. J Exp Med 2014;211 (6):1153–66.
[48] Katakai T, Hara T, Lee JH, Gonda H, Sugai M, Shimizu A. A novel reticular stromal structure in lymph node cortex: an immuno-platform for interactions among dendritic cells, T cells and B cells. Int Immunol 2004;16(8):1133–42.
[49] Arngrim N, Simonsen L, Holst JJ, Bulow J. Reduced adipose tissue lymphatic drainage of macromolecules in obese subjects: a possible link between obesity and local tissue inflammation?. Int J Obes (Lond) 2013;37(5):748–50.

[50] Movat HZ, Fernando NV. The Fine Structure of Lymphoid Tissue. Exp Mol Pathol 1964;3:546–68.
[51] Crivellato E, Mallardi F. Stromal cell organisation in the mouse lymph node. A light and electron microscopic investigation using the zinc iodide-osmium technique. J Anat 1997;190(Pt 1):85–92.
[52] Han SS. The ultrastructure of the mesenteric lymph node of the rat. Am J Anat 1961;109:183–225.
[53] Takeuchi A, Ozawa M, Kanda Y, Kozai M, Ohigashi I, Kurosawa Y, et al. A Distinct Subset of Fibroblastic Stromal Cells Constitutes the Cortex-Medulla Boundary Subcompartment of the Lymph Node. Front Immunol 2018;9:2196.
[54] Kuka M, Iannacone M. The role of lymph node sinus macrophages in host defense. Ann N Y Acad Sci 2014;1319:38–46.
[55] Merkel M, Eckel RH, Goldberg IJ. Lipoprotein lipase: genetics, lipid uptake, and regulation. J Lipid Res 2002;43(12):1997–2006.
[56] Lichtenstein L, Mattijssen F, de Wit NJ, Georgiadi A, Hooiveld GJ, van der Meer R, et al. Angptl4 protects against severe proinflammatory effects of saturated fat by inhibiting fatty acid uptake into mesenteric lymph node macrophages. Cell Metab 2010;12(6):580–92.
[57] Aterman K, Remmele W, Karl Smith M. Touton and his ‘‘xanthelasmatic giant cell.” A selective review of multinucleated giant cells. Am J Dermatopathol 1988;10(3):257–69.